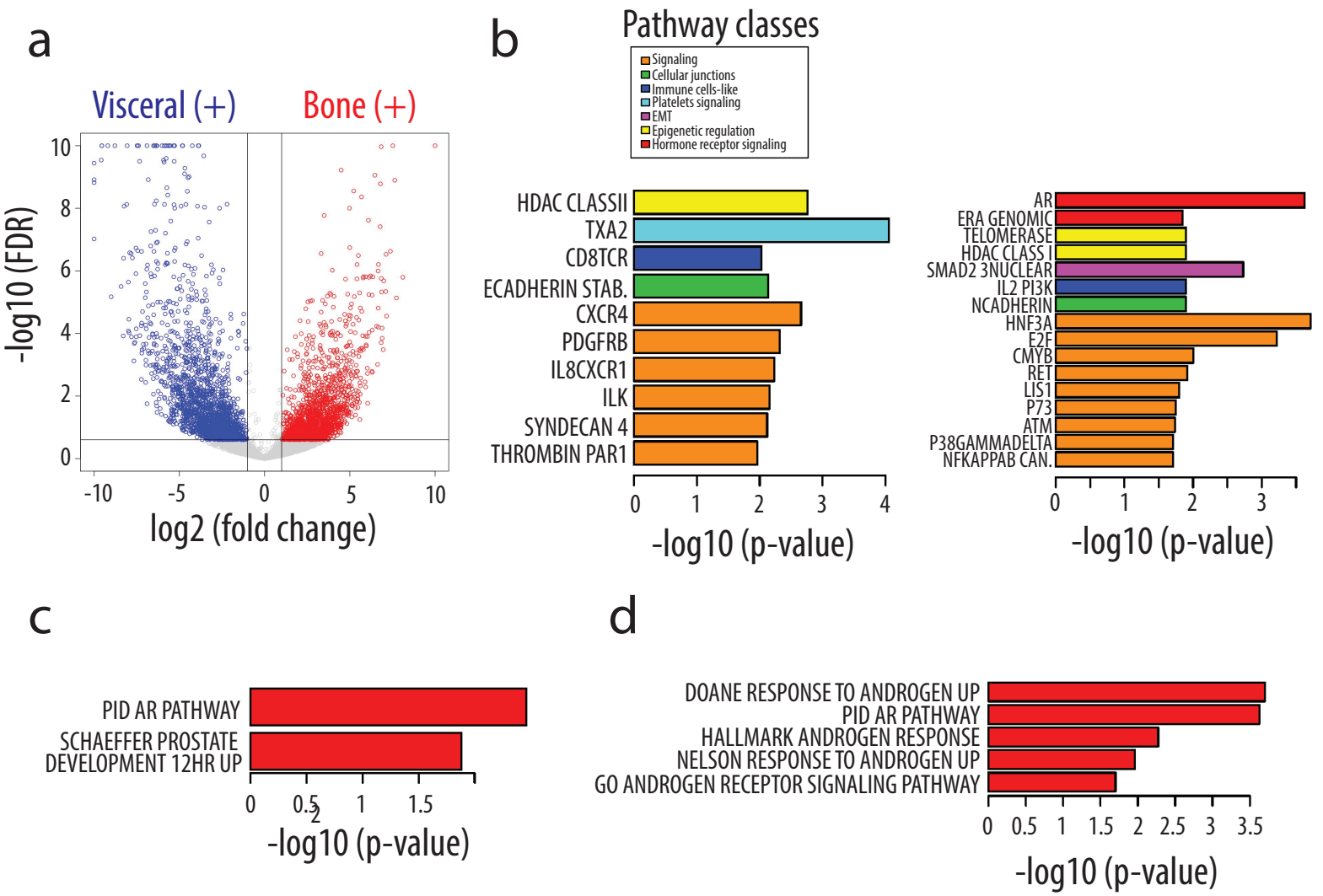

Figure S1. RNA sequencing and pathway analysis of CTCs from Bone(+) versus Visceral(+) breast cancer patients. a) Volcano plot showing the fold change versus false discovery rate (FDR) for each individual gene in CTCs from patients with Bone(+) versus Visceral(+) metastasis. Differently from Fig 1b, this analysis takes into account individual samples and without pooling samples by patient. **b)** Bar graph showing all significantly enriched pathways (FDR<0.25) using PID tool in CTCs from Bone(+) versus Visceral(+) patients. Pathways are grouped into seven classes. Differently from Fig 1c, this analysis takes into account individual samples and without pooling samples by patient. **c)** Bar graph showing singnificantly enriched signatures (FDR<0.25) using MSigDB tool, filtering for signatures describing AR activation, in CTCs from Bone(+) patients. This analysis is conducted by pooling CTCs derived from the same patient. **d)** Bar graph showing singnificantly enriched signatures (FDR<0.25) using MSigDB tool, filtering for signatures describing in AR activation, in CTCs from Bone(+) patients. This analysis is conducted in individual samples and without pooling samples by patient.

FIGURE S1 Aceto et al.

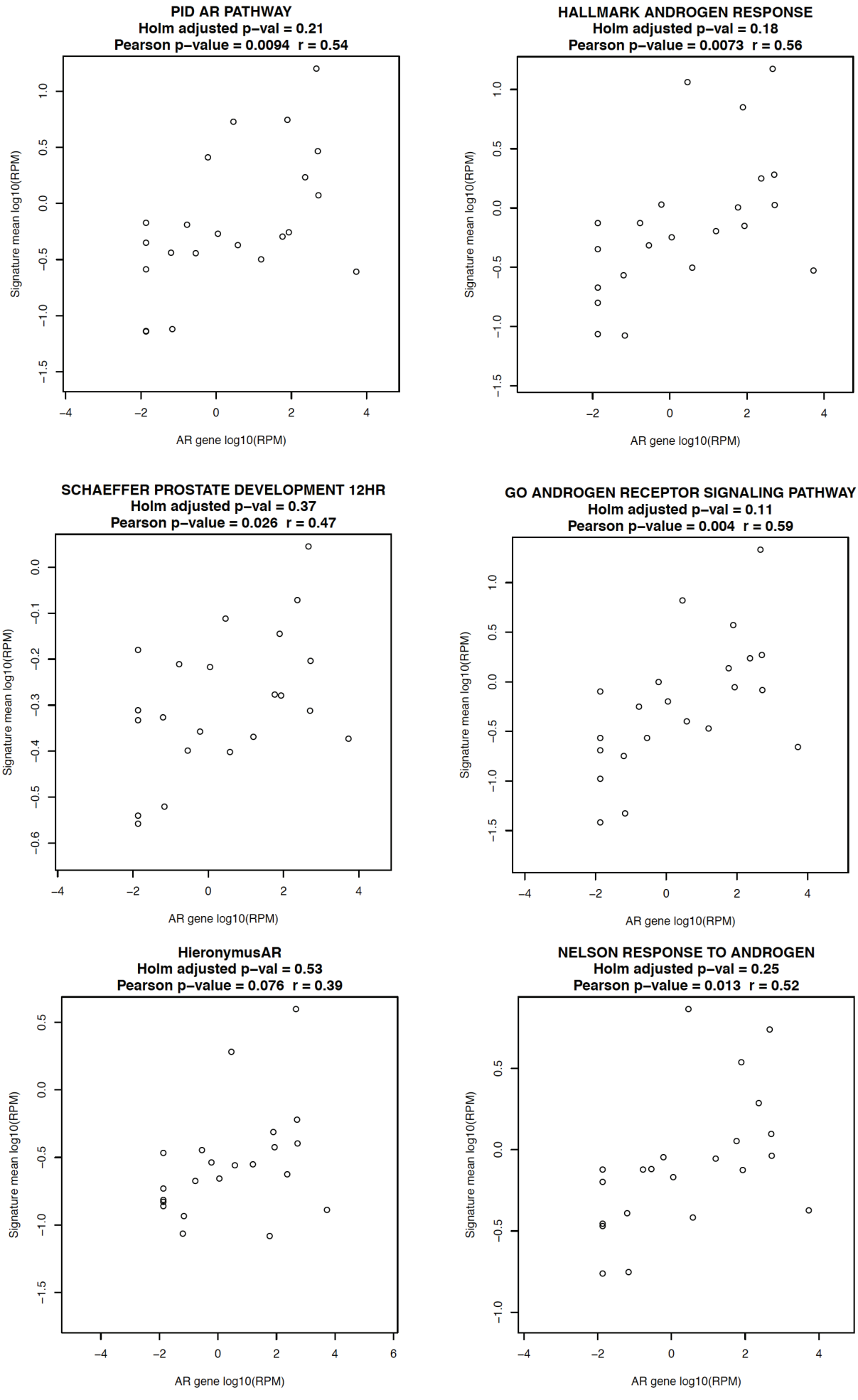

Figure S2. Correlation between AR expression and AR signatures. Correlation plots displaying the relationship between AR gene expression in our CTC samples and activation of various AR signatures from different databases. Signature names and p-values are shown above each plot.

FIGURE S2 Aceto et al.

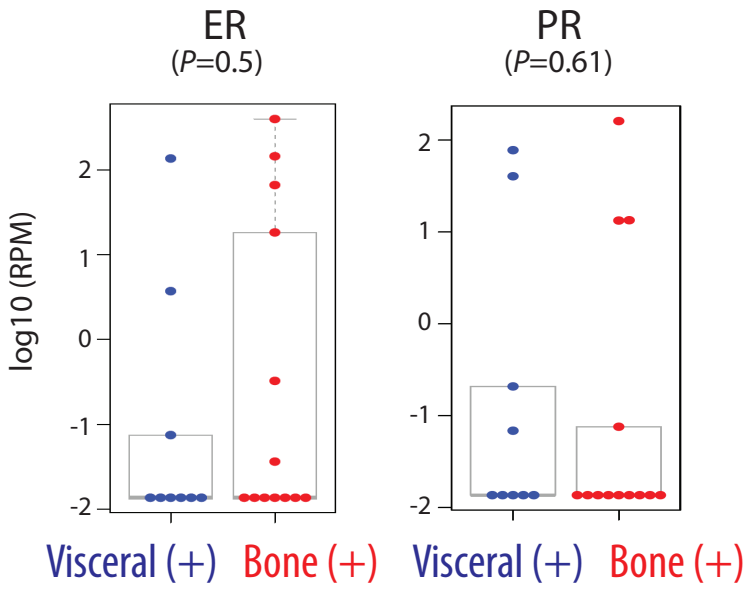

Figure S3. ER and PR expression in CTCs from Bone(+) versus Visceral(+) breast cancer patients. Boxplots show ER and PR transcript expression levels in CTCs from patients with "progressing bone metastasis" (red) versus "Progressing Visceral + Soft tissue" metastasis (blue). Reads per million (rpm) are averaged by patient. p values are given within parenthesis.

FIGURE S3 Aceto et al.

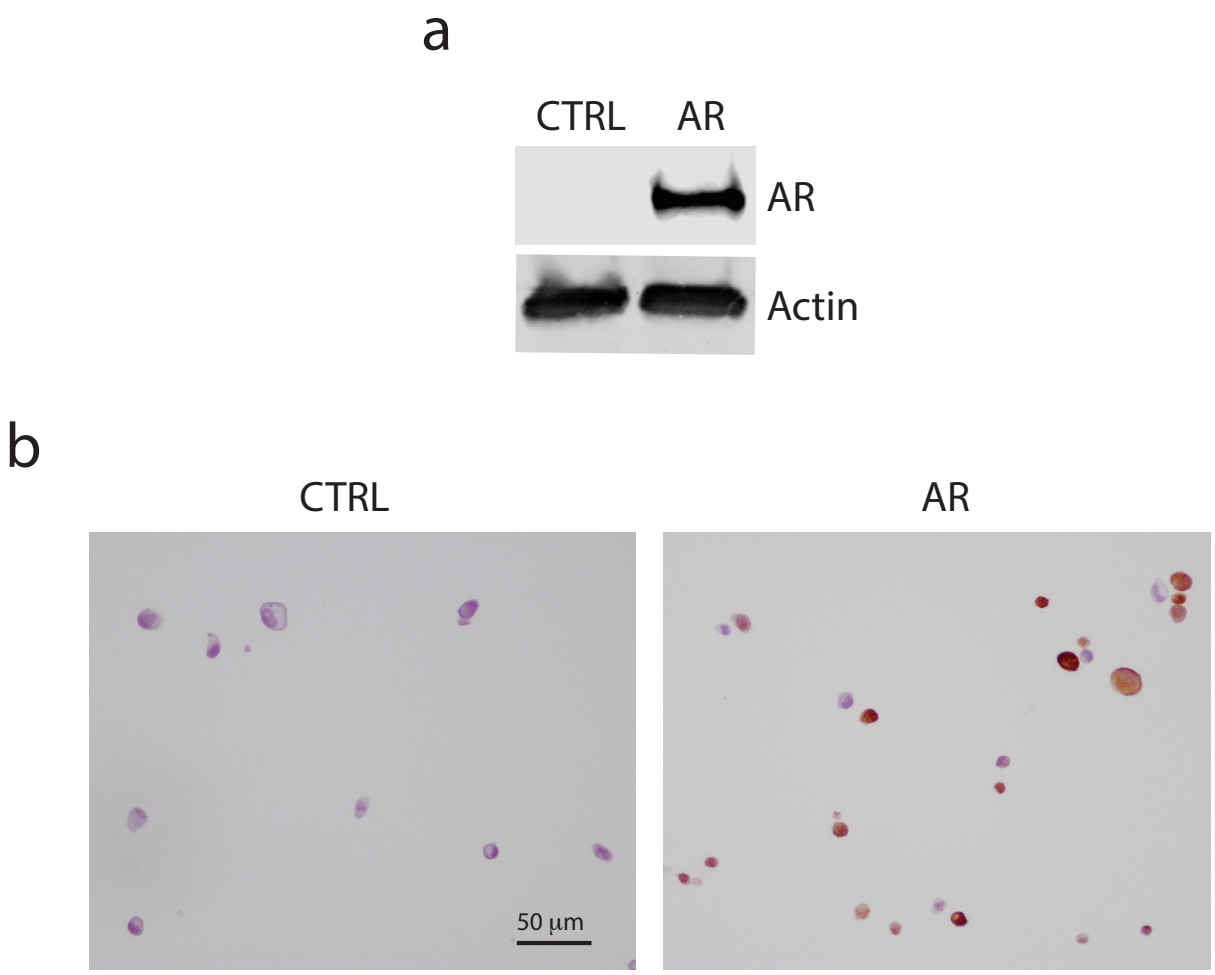

Figure S4. AR antibody validation. a) Immunoblot showing the androgen receptor (AR) expression in MDA-MB-231 cells transduced with a control vector (CTRL) or a human AR expression vector. **b**) Representative images of sections from paraffin-embedded MDA-MB-231 cells transduced with a control vector (CTRL) or a human AR expression vector and stained with anti-AR antibodies.

FIGURE S4 Aceto et al.

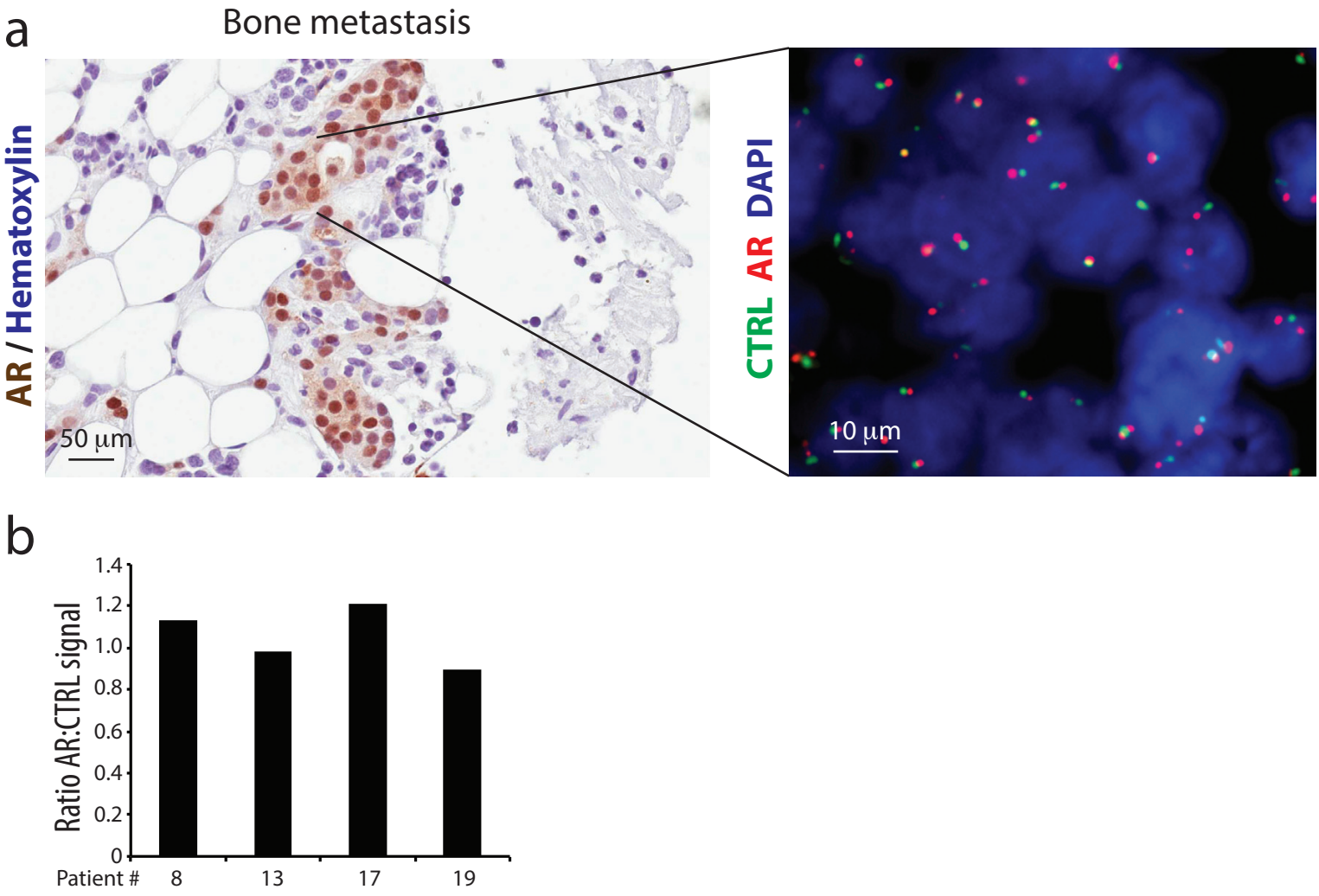

Figure S5. AR copy number assessment in breast cancer bone metastasis. a) Representative images of AR (brown) and hematoxylin (blue) stains (left) and the corresponding fluorescence in situ hybridization analysis of AR copy number (right) in bone metastasis from a breast cancer patient. **b**) The bar graph shows the ratio of AR:CTRL signal in the four bone metastases known to overexpress AR.

FIGURE S5 Aceto et al.

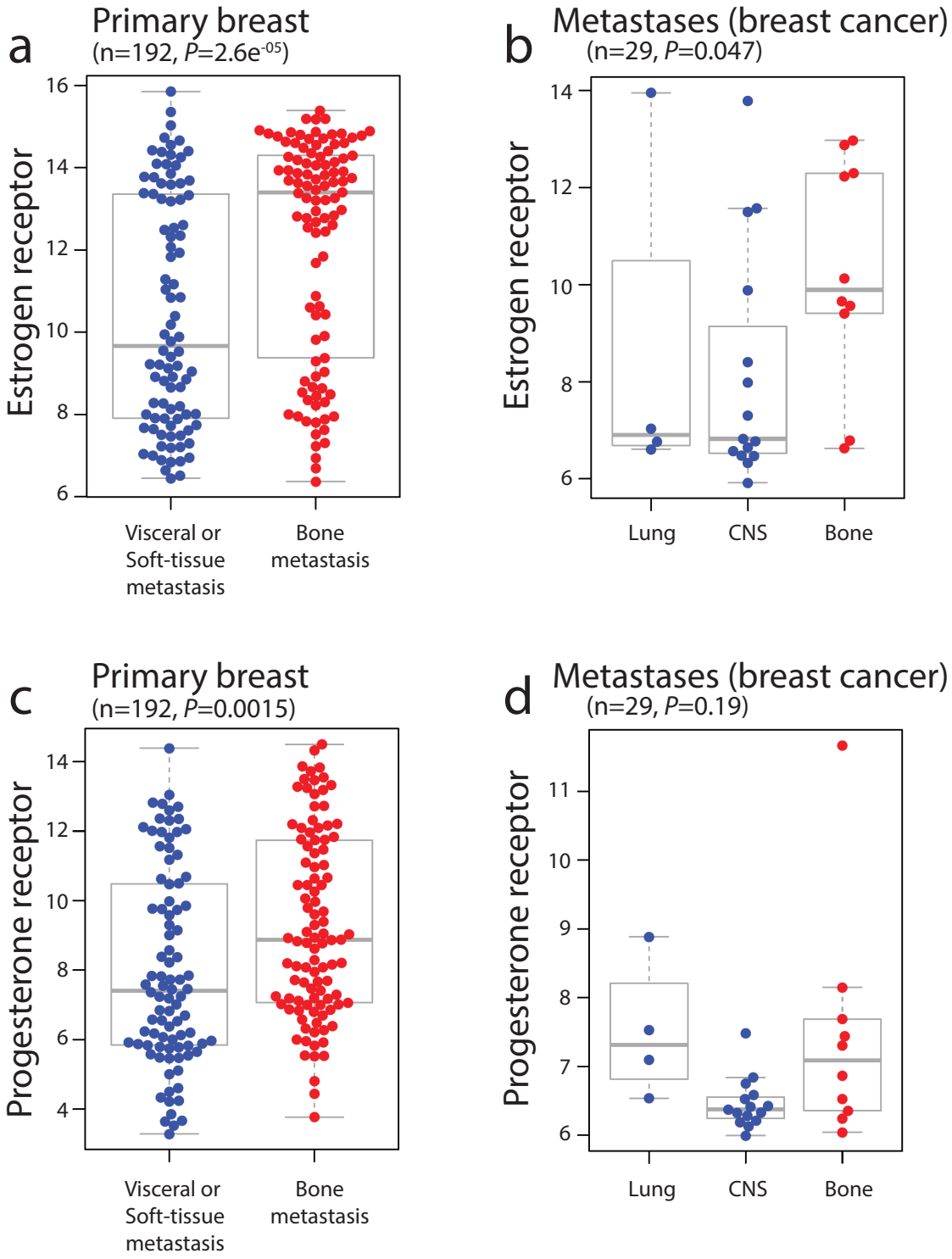

Figure S6. ER and PR expression in primary and metastatic breast cancer. a) Boxplot showing estrogen receptor (ER) expression in human primary breast tumors (n=192, *left*) from patients who later devloped metastasis in the bone versus other organs. *P* values are shown within parentheses. **b**) Boxplot showing ER expression in biopsies of breast cancer metastases in the lung, liver or bone of patients (n=29). *P* value is shown within parentheses. **c**) Boxplot showing progesterone receptor (PR) expression in primary breast tumors (n=192, *left*) from patients who later developed metastasis in the bone versus other organs. *P* values are shown within parentheses. **d**) Boxplot showing PR expression in biopsies of breast cancer metastasis in the lung, liver or bone of patients (n=29). *P* value is shown within parentheses.

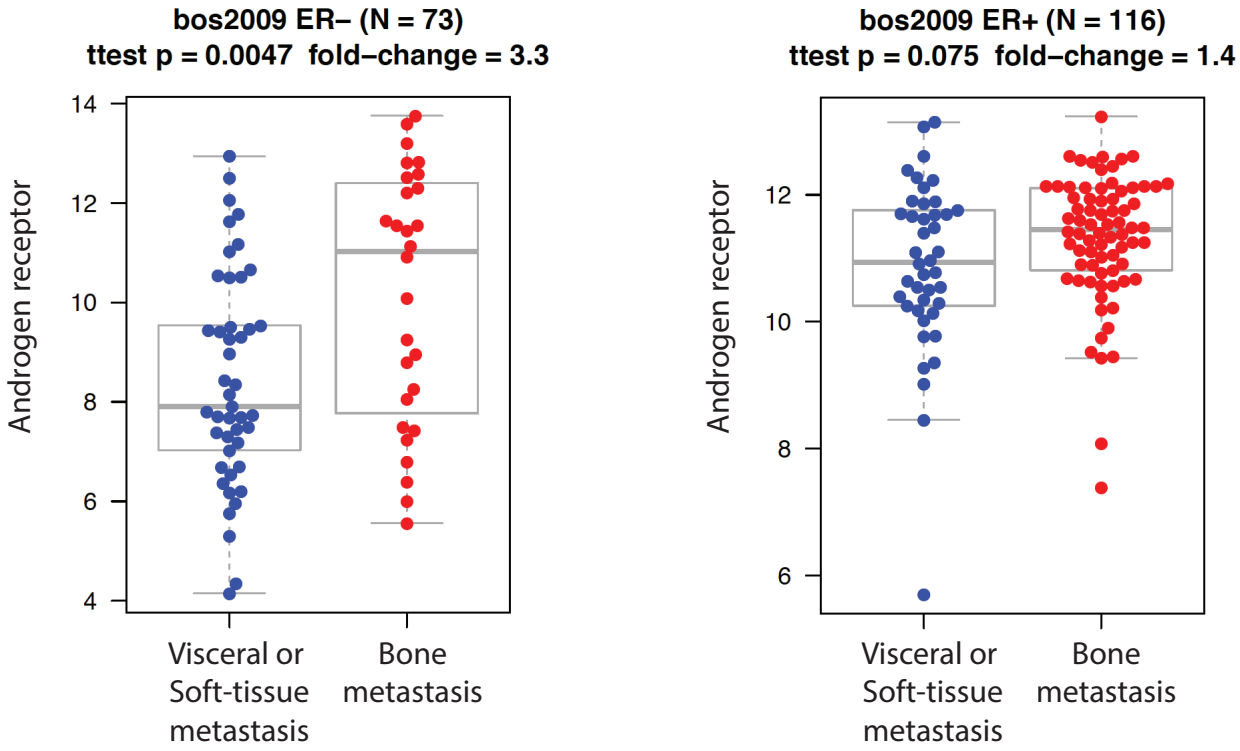

Figure S7. AR expression correlates with bone metastasis independently of ER status. Boxplots showing AR expression levels in primary breast tumors (n=192; Bos et al, Nature 2009) from patients who later developed metastasis in the bone versus other organs. The left plot represents patients with ER negative tumor, while the right plots represents patients with ER positive tumor.

FIGURE S7 Aceto et al.

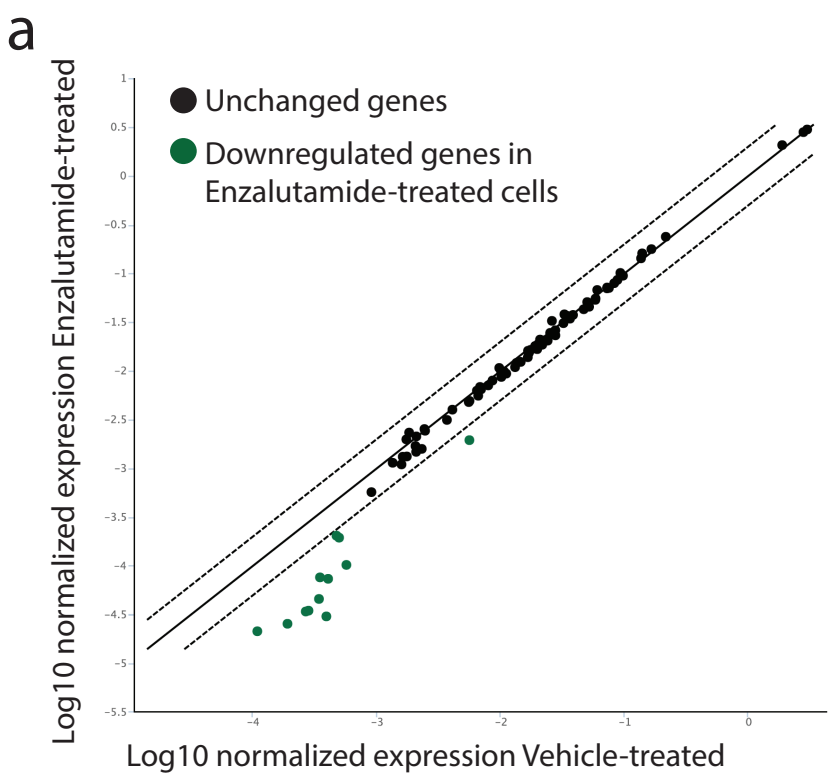

Figure S8. Enzalutamide treatment induces downregulation of a subset of AR-dependent genes in breast cancer cells. a) Plot showing the mRNA expression levels of a setof androgen receptor (AR) target genes (see methods section) in MDA-MB-231-Bo cells treated with Enzalutamide or Vehicle. Genes that are downregulated as a consequence to Enzalutamide treatment in MDA-MB-231-Bo cells are shown in green ($P<0.05$). **b)** IDs of downregulated genes are shown.

FIGURE S8 Aceto et al.

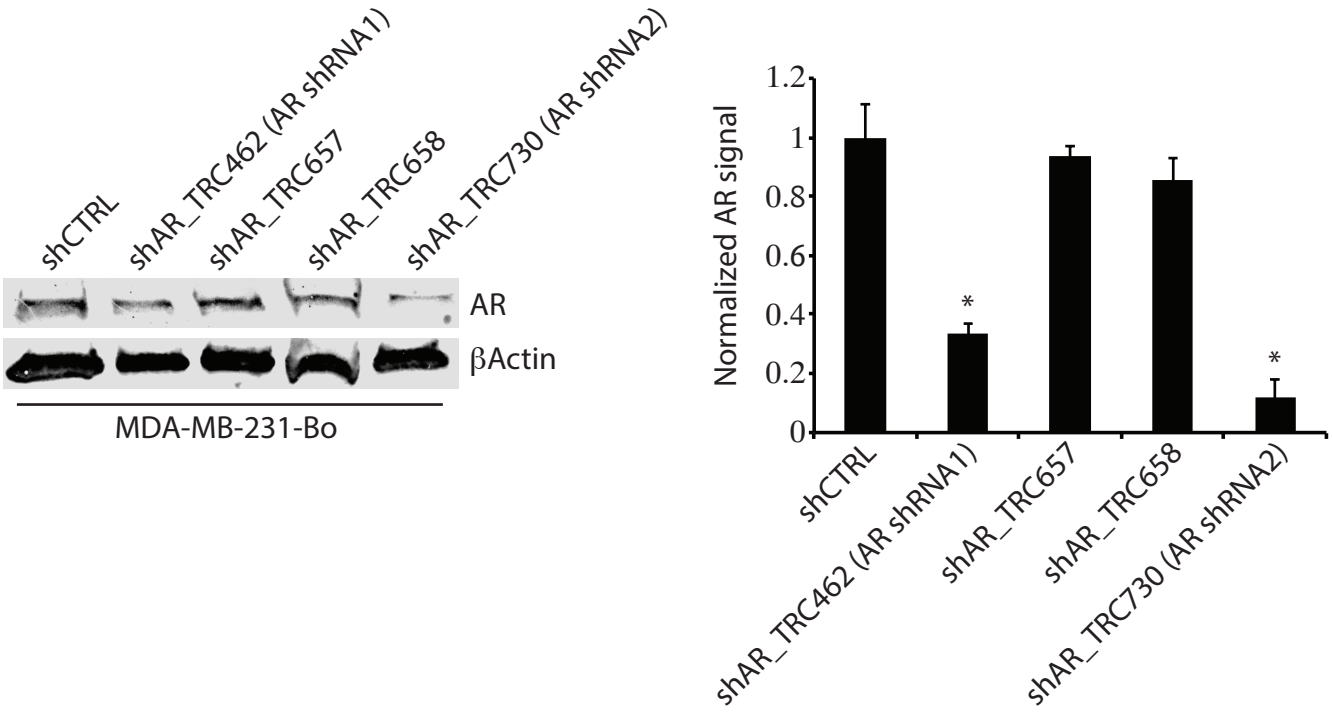

Figure S9. AR shRNA validation. Immunoblot showing the expression levels of androgen receptor (AR) in MDA-MB-231-Bo cells expressing two different shRNAs targeting the AR (*left*). The bar graph shows the normalized AR band intensity for each lane (*right*). n=3. P<0.006.

FIGURE S9 Aceto et al.

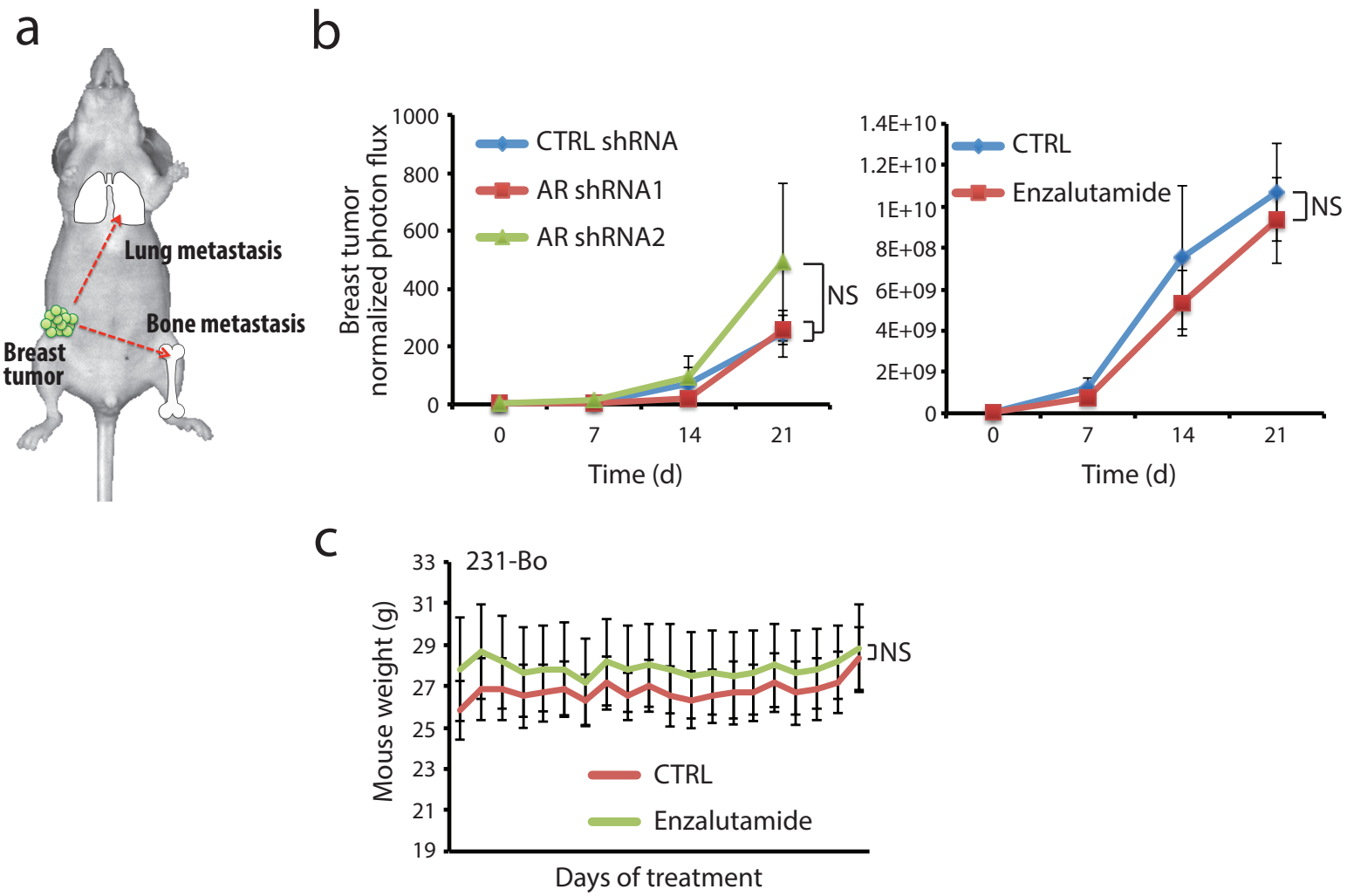

Figure S10. AR inhibition does not alter primary tumor growth. a) Schematic of the experiment: MDA-MB-231-Bo cells labeled with GFP-Luciferase were injected into the mammary fat pad of mice. **b**) Curves show the tumor growth from MDA-MB-231-Bo cells labeled with GFP-Luciferase and expressing either a control or AR shRNAs (*left*). Curves show the tumor growth from MDA-MB-231-Bo cells labeled with GFP-Luciferase and treated with vehicle or enzalutamide (*right*). **c**) Curves show the mean mouse weight during enzalutamide treatment. NS= not significant.

FIGURE S10 Aceto et al.